# Secular change in atmospheric Ar/N₂ and its implications for ocean heat uptake and Brewer-Dobson circulation

Shigeyuki Ishidoya[1], Satoshi Sugawara[2], Yasunori Tohjima[3], Daisuke Goto[4], Kentaro Ishijima[5], Yosuke Niwa[3], Nobuyuki Aoki[1] and Shohei Murayama[1]

5   [1]National Institute of Advanced Industrial Science and Technology (AIST), Tsukuba 305-8569, Japan
[2]Miyagi University of Education, Sendai 980-0845, Japan
[3]National Institute for Environmental Studies, Tsukuba 305-8506, Japan
[4]National Institute of Polar Research, Tokyo 190-8518, Japan
[5]Meteorological Research Institute, Tsukuba 305-0052, Japan

10   *Correspondence to*: Shigeyuki Ishidoya (s-ishidoya@aist.go.jp)

**Abstract.** Systematic measurements of the atmospheric Ar/N₂ ratio have been made at ground-based stations in Japan and Antarctica since 2012. Clear seasonal cycles of the Ar/N₂ ratio with summertime maxima were found at middle to high latitude stations, with seasonal amplitudes increasing with increasing latitude. Eight years of the observed Ar/N₂ ratio at Tsukuba and Hateruma, Japan showed not only secular increasing trends, but also interannual variations in phase with the

15   observed variations in the global ocean heat content (OHC). The observed secular trend of the Ar/N₂ ratio was $0.75\pm0.30$ per meg $yr^{-1}$. Sensitivity test by using a 2-dimensional model with the Brewer-Dobson circulation (BDC) scenarios indicated the possibility of the secular trend in the surface Ar/N₂ ratio being modified significantly by the gravitational separation in the stratosphere. The secular trend of the Ar/N₂ ratio, corrected for gravitational separation under the assumption of weakening of BDC simulated by the 2D model, was $0.60\pm0.30$ per meg $yr^{-1}$. By using a conversion factor of $3.5\times10^{-23}$ per meg $J^{-1}$ by

20   assuming a 1-box ocean with a temperature of 3.5 °C, then an average OHC increase rate of $17.1\pm8.6$ ZJ $yr^{-1}$ for the period 2012 – 2019 was estimated from the corrected secular trend of the Ar/N₂ ratio. This value is consistent with $12.2\pm1.2$ ZJ $yr^{-1}$ reported by ocean temperature measurements. The effect of the actual atmospheric circulation on the Ar/N₂ ratio is still unclear, however the analytical results obtained in the present study imply that the surface Ar/N₂ ratio is an important tracer for detecting spatiotemporally-integrated changes in OHC and BDC.

25

## 1 Introduction

The Ar/N₂ ratio of air is a unique tracer for detecting changes in the spatiotemporally-integrated air-sea heat flux or ocean heat content (OHC). This is because variations in the Ar/N₂ ratio at the Earth's surface are driven by air-sea Ar and N₂ fluxes that reflect changes in the solubility of these gases in seawater (e.g. Keeling et al., 2004). The increase in the global OHC is

30   one of the most important parameters for evaluating earth's climate system (e.g. Trenberth and Fasullo, 2010). The relative temperature dependence of the solubility of Ar is larger than that of N₂, so that the atmospheric Ar/N₂ ratio increases with

increasing ocean temperature. Other noble gases behave in a similar way. Bereiter et al. (2018), for example, analyzed $Kr/N_2$ and $Xe/N_2$ ratios in air trapped in ice cores and estimated that the mean global ocean temperature increased by 2.57±0.24 °C over the last glacial transition (20,000 to 10,000 years ago). In terms of ocean heat content, the present-day global OHC

35 increase is evaluated from analysing the ocean temperature measurements using Argo float (e.g. Cheng et al., 2019). Therefore, precise measurements of the $Ar/N_2$ ratio in air can be used as an independent validation of the OHC estimation from the ocean data. However, long-term changes in the atmospheric $Ar/N_2$ ratio have never been reported so far due to difficulties in detecting a trend with sufficient accuracy, although a few past studies observed its seasonal variations (Keeling et al., 2004; Blaine, 2005; Cassaer et al., 2008; Ishidoya and Murayama, 2014).

40 We have reported in past studies that the $Ar/N_2$ ratio decreases with increasing altitude in the stratosphere due to gravitational separation of the atmospheric constituents (e.g. Ishidoya et al., 2013; Sugawara et al., 2018). The magnitude of gravitational separation is determined by a balance between mass-independent atmospheric transport, that is, advection and eddy diffusion, and mass-dependent molecular diffusion in the atmosphere. This implies that gravitational separation will be influenced by the atmospheric circulation changes. Therefore, we can use the observed gravitational separation as an

45 indicator of the Brewer-Dobson circulation (BDC) in the stratosphere. There has been no study to evaluate the effect of gravitational separation changes in the stratosphere on the concentrations and isotopic ratios of atmospheric trace gases at the surface, since it has been believed that the gravitational separation near the surface is too small to be detected and thus unquestionably negligible. Therefore, in our previous studies, we simulated "δ", which is an indicator of gravitational separation derived from the $Ar/N_2$ ratio and stable isotopic ratios of $N_2$, $O_2$ and Ar, using atmospheric transport models by

50 assuming the surface δ to be zero (Ishidoya et al., 2013; Sugawara et al., 2018; Belikov et al., 2019). However, because long-term changes in the $Ar/N_2$ ratio near the surface is expected to be extremely small, e.g. 0.00026 % corresponding to a heat input of 100 ZJ (1 zetajoule = $10^{21}$ J) into a 10 °C ocean (Keeling et al., 2004), a very small secular change in gravitational separation near the surface may modify the long-term change in the surface $Ar/N_2$ ratio. If so, an evaluation of gravitational separation of the whole atmosphere is needed for a precise estimate of the global OHC increase based on long-term changes

55 in the surface atmospheric $Ar/N_2$ ratio.

In this paper, we present results from an analysis of 8-year-long measurements of the atmospheric $Ar/N_2$ ratio at the ground surface stations and propose "$\delta_\Omega$" as a new indicator of gravitational separation of the whole atmosphere by using a 2-D model. By using the simulated $\delta_\Omega$, we derived the secular trend of $Ar/N_2$ ratio corrected for gravitational separation changes associated with the BDC change. Finally, we estimated the global OHC change based on the corrected $Ar/N_2$ ratio.

## 60 2 Experimental procedures

Atmospheric $Ar/N_2$ ratio has been observed at Tsukuba (TKB; 36°N, 140°E), Japan continuously since February 2012 (Ishidoya and Murayama, 2014). Located on the roof of a laboratory building of the National Institute of Advanced Industrial Science and Technology (AIST), sample air is taken from an air intake by using a diaphragm pump with gas

velocity higher than 5 ms$^{-1}$ (4 mm ID and a flow rate of 4 L min$^{-1}$) at the tip of the air intake to prevent thermally-diffusive

65    inlet fractionation (Sturm et al., 2006; Blaine et al., 2006). The sample air is introduced into a 1 L stainless steel buffer tank

after water vapour in the air is reduced by using an electric cooling unit at 2°C. The gas is then exhausted from the buffer

tank at a flow rate of about 4 L min$^{-1}$. A small portion of this exhausted gas is introduced into a 1/8-inch OD stainless-steel

tube and any remaining water vapour is removed using a cold trap at -90 °C. Finally, the remaining sample air is vented

through an outlet path at a rate of about 10 mL min$^{-1}$, and only a miniscule amount of it is transferred to the ion source (or

70    waste line) of a mass spectrometer (Thermo Scientific Delta-V) through an insulated thin fused-silica capillary. As for the

reference air, it is always supplied from a high-pressure cylinder at a flow rate of about 4 mL min$^{-1}$, and a miniscule amount

of it is introduced into the ion source (or waste line) of the mass spectrometer through another fused-silica capillary. For the

continuous measurements, alternate analyses of the sample and reference air are made repeatedly. The measurement time

required to obtain one data value is 62 seconds, and we usually use 550-data averaged value as Ar/N$_2$ ratio obtained from the

75    continuous observations (about 11 hours averaged value). We also measure stable isotopic ratios of N$_2$, O$_2$ and Ar, and O$_2$/N$_2$

ratio and CO$_2$ mole fraction simultaneously, and use the 550-data averaged values for the stable isotopic ratios and one data

value without averaging for O$_2$/N$_2$ ratio and CO$_2$ mole fraction; these measurements constitute the continuous observations.

Details of the continuous measurement system used are given in Ishidoya and Murayama (2014).

We have also collected air samples at a rate of once per month at Hateruma Island (HAT; 24°N, 124°E) and Cape Ochiishi

80    (COI; 43°N, 146°E), Japan since July 2012 and October 2013, respectively, and at Syowa station (SYO; 69°S, 40°E) since

January 2016, for the analyses of the atmospheric Ar/N$_2$ ratio. Each air sample is taken from an air intake by using a

diaphragm pump at a flow rate of about 5 L min$^{-1}$ and filled into a 1 L stainless steel flask whose inner walls are silica-coated

after removing water vapour using a cold trap (-40 °C at HAT and COI, and -80 °C at SYO). Similar to our previous study

(Ishidoya et al., 2016), the 1 L stainless steel flasks are equipped with two metal-seal valves on each side to equalize the

85    inner pressure to the pressure between the two metal-seal valves to prevent a mass-dependent fractionation due to small leak

through the valve. During air sampling, the inner pressure of the flask is kept at an absolute pressure of 0.2 MPa using a

backpressure valve (Tohjima et al., 2003). The sample air collected in the flasks are then sent to AIST and analyzed by using

the same mass spectrometer as described above. The sample air is supplied from the flask at a flow rate of about 4 mL min$^{-1}$

through a cold trap (about -50 °C), and a miniscule amount of it is introduced into the ion source (or waste line) of the mass

90    spectrometer through a fused-silica capillary. It is noted that we also used 760 mL glass flasks with a Viton O-ring seal

valves on each side for collecting air samples at HAT and COI prior to September, 2015 and January, 2019, respectively.

However, we found slight seasonally dependent differences in the Ar/N$_2$ and O$_2$/N$_2$ ratios between the analytical results from

the 1 L stainless steel flasks and those from the 760 mL glass flasks. It is interesting to note that the O$_2$/N$_2$ ratio from the 1 L

stainless steel flasks agree well with the O$_2$/N$_2$ ratio reported by the National Institute for Environmental Studies (NIES) (e.g.

95    Tohjima et al., 2019), considering the difference in the span sensitivity of the O$_2$/N$_2$ ratio between the AIST and NIES (our

unpublished data). Therefore, we have decided to adopt the Ar/N$_2$ data obtained from the 1 L stainless steel flasks and

correct the data from the 760 mL glass flasks based on the comparison of the Ar/N$_2$ ratios measured from the stainless steel

flasks and the glass flasks at HAT for the period October, 2015 – January, 2019. Cause(s) of such an offset between the stainless steel flasks and glass flasks have not been determined yet, but it may be related to the seasonal difference in the
100    ambient temperature during the time the flasks were shipped from the observational sites to our laboratory and its effect on the condition of Viton O-ring seal valves used in the glass flask.

The Ar/$N_2$ ratio is usually reported in per meg unit as follows.

$$\delta(Ar/N_2) = \left( \frac{\left( [n_{Ar}]/[n_{N_2}] \right)_{sample}}{\left( [n_{Ar}]/[n_{N_2}] \right)_{standard}} - 1 \right) \times 10^6. \qquad (1)$$

Here, the subscripts 'sample' and 'standard' indicate the sample air and the standard gas, respectively. Because Ar
105    constitutes 9,334 $\mu$mol mol$^{-1}$ of air by volume (Aoki et al., 2019), 5 per meg of $\delta(Ar/N_2)$ is equivalent to about 0.05 $\mu$mol mol$^{-1}$. In this study, $\delta(Ar/N_2)$ of each air sample was determined against our primary standard air (cylinder No. CRC00045) using the mass spectrometer Thermo Scientific Delta-V. Our air standards, which are classified into primary and secondary, are dried ambient air or industrially-purified air-based $CO_2$ standard filled in 48-L high-pressure cylinders. As shown in Fig. 1, variations in the annual average $\delta(Ar/N_2)$ of our 3 secondary standards are within $\pm 0.9 - \pm 2.2$ per meg ($\pm 1.6$ per meg, on
110    average) and nearly stable for 8 years with respect to the primary standard. Therefore, we allowed an uncertainty of $\pm 1.6$ per meg for the annual average $\delta(Ar/N_2)$ observed in the present study associated with the stability of the standard air, which corresponds to the uncertainty of $\pm 0.28$ per meg yr$^{-1}$ for the 8-year-long secular trend. We have also prepared high-precision gravimetric standard mixtures of Ar, $O_2$, $N_2$ and $CO_2$, with standard uncertainties for the Ar and $O_2$ molar fractions of 0.6 to 0.8 $\mu$mol mol$^{-1}$ (Aoki et al., 2019). From the measurements of the gravimetrically-prepared standard mixtures by the mass
115    spectrometer, it was confirmed that the span sensitivity of $\delta(Ar/N_2)$ obtained from the mass spectrometer agreed to within 0.2 % of the gravimetric values of the standard mixtures, in the range from -4,500 to 1,800 per meg of $\delta(Ar/N_2)$ against our primary standard air.

In the present study, we use 1-week averaged values from the continuous observation at Tsukuba after implementing the following data selection procedure. First, the $\delta(Ar/N_2)$ values with $\delta^{15}N$ higher than 3.0 per meg were excluded from the
120    analyses. As mentioned above, the $\delta(Ar/N_2)$ and $\delta^{15}N$ values are already 11-hour averaged values. We have found these high $\delta^{15}N$ events accompanied by high $CO_2$ events, as well as occasionally with slightly high $\delta(Ar/N_2)$ events, especially in the winter, but did not correlate with variations in the isotopic ratio of $O_2$ and Ar. Therefore, it appears that some unspecified interferences of mass 29 (possibly $^{13}C^{16}O$ and/or fragments of hydrocarbons) rather than the molecular-diffusive separation of $^{15}N^{14}N$ and $^{14}N^{14}N$ must have superimposed on the observational results of $\delta^{15}N$ during these events. It is possible that
125    these high $CO_2$ and $\delta^{15}N$ events occur under a stable atmospheric condition in the winter, so that simultaneously observed $\delta(Ar/N_2)$ may also be modified by local effects such as thermally-diffusive separation of Ar and $N_2$ due to temperature inversion near the surface (Adachi et al., 2006). Therefore, the threshold value of 3.0 per meg was determined to be

reasonable, considering that an average $\delta^{15}N$ value of 1.1±1.7 per meg was observed at HAT for the period October 2015 – January 2020, while the observed $CO_2$ mole fractions over the same period were much closer to the values of the background

130 air than those observed at TKB. After the above data selection procedure, 1-week averaged values of $\delta(Ar/N_2)$ were calculated. The measurement uncertainty of the 1-week averaged values of the continuous observation was estimated to be about ±3 per meg as a standard deviation from the best-fit curve (see Fig. 2 in 3-1), while that of the flask air sample measurements was estimated to be about ±7 per meg from repeated analyses of the same air samples.

## 3 Results and discussion

135 ### 3.1 Atmospheric $\delta(Ar/N_2)$ observed at ground surface stations in Japan and Antarctica

Figure 2 shows atmospheric $\delta(Ar/N_2)$ observed at COI, TKB, HAT and SYO. Best-fit curves to the data and long-term trends obtained using a digital filtering technique (Nakazawa et al., 1997) are also shown. In this filtering technique, the average seasonal cycles of $\delta(Ar/N_2)$ are approximated by fundamental and its first harmonics, and signals with periods longer than 36 months were regarded as contributing to a long-term trend. As seen in Fig. 2, we can distinguish clear

140 seasonal $\delta(Ar/N_2)$ cycles at COI, TKB and SYO and some interannual variations in the long-term trend at TKB and HAT. Figure 3 shows the detrended values of $\delta(Ar/N_2)$ and average seasonal $\delta(Ar/N_2)$ cycles observed at all 4 sites. The seasonal maxima were found in the summertime, which is expected since the sea surface temperatures around the observational sites reach seasonal maximum in the summertime, enhancing the larger relative temperature dependent solubility of Ar compared to that of $N_2$. The peak-to-peak amplitudes of the seasonal $\delta(Ar/N_2)$ cycles were 21±10, 11±4, 5±10 and 32±9 per meg at

145 COI, TKB, HAT and SYO, respectively. The uncertainties for the amplitudes indicate standard deviations of the detrended values from the average seasonal cycle. Similar increase in the seasonal $\delta(Ar/N_2)$ cycle amplitude with increasing latitude were also observed by Keeling et al. (2004) and Cassar et al. (2008). Cassar et al. (2008) also reported on the seasonal $\delta(Ar/N_2)$ cycle at SYO with a peak-to-peak amplitude of 21±8 per meg. The amplitude at SYO found in this study is consistent with that found by Cassar et al. (2008), within the quoted uncertainties. For La Jolla (LJO; 33°N, 117°W), USA

150 located at a similar latitude as TKB, Keeling et al. (2004) and Blaine (2005) found seasonal $\delta(Ar/N_2)$ cycle with a peak-to-peak amplitude of about 10 per meg. This agrees with the amplitude at TKB observed in this study. Seasonal minima and maxima at SYO and LJO reported by Cassar et al. (2008) and Keeling et al. (2004), respectively, are in general agreement with those observed at SYO and TKB in this study. On the other hand, the seasonal $\delta(Ar/N_2)$ cycle at HAT was not so clear but the average peak-to-peak amplitude may be slightly smaller than 14±6 per meg observed at Kumukahi (20°N, 155°W),

155 USA located at a similar latitude to HAT (Keeling et al., 2004). Similar and consistent results obtained by this and other studies give confidence in our ability to capture natural variations of $\delta(Ar/N_2)$ in the atmosphere.

Figure 4 shows variations in $\delta(Ar/N_2)$ observed at TKB and HAT, after subtracting seasonal cycles and shorter-term variations of less than 36 months. For analyses of the long-term trends, we used only the data from TKB and HAT since the

observations at these stations date back to 2012 and are longer than data from other sites. Variations in the 0-2000 m global
160   OHC reported by the National Oceanographic Data Center (NOAA)/National Centers for Environmental Information
(NCEI) (updated from Levitus et al. 2012, https://www.nodc.noaa.gov/OC5/3M_HEAT_CONTENT/) and their long-term
trends obtained by using the same digital filtering technique used in Fig. 2, and globally averaged surface temperature
anomalies (Japan Meteorological Agency, http://www.data.jma.go.jp/cpdinfo/temp/nov_wld.html) are also shown. Increase
rates of the long-term trends of $\delta(Ar/N_2)$ and OHC are also shown by red lines. As can be seen from the figure, $\delta(Ar/N_2)$
165   show significant interannual variations and slight secular increases while the global OHC show a more prominent secular
increase. Moreover, interannual variations in the increase rates of $\delta(Ar/N_2)$ and OHC are quite similar to each other in phase,
suggesting a strong correlation between the large-area air-sea heat flux and the long-term change in $\delta(Ar/N_2)$. The minima of
the increase rates of $\delta(Ar/N_2)$ and OHC appeared at the beginning of 2016 when a maximum in the surface temperature
anomaly appeared. This correspondence is qualitatively reasonable since a decrease in the OHC increase rate indicates a
170   decrease in the net ocean heat uptake, and thus leading to an increase in surface temperature.

As mentioned above, the ratio of interannual variation to secular increase is larger for $\delta(Ar/N_2)$ than for OHC. To examine
this difference, we estimated the interannual variation of the atmospheric $\delta(Ar/N_2)$ expected from the air-sea Ar and $N_2$
fluxes caused by the interannual variation in the global OHC. We converted the increase rate of OHC to that of $\delta(Ar/N_2)$ by
assuming a coefficient of $3.5\times10^{-23}$ or $3.0\times10^{-23}$ per meg $J^{-1}$, which was derived from the following equations (Keeling et al.,
175   1993).

$$F_{Ar} = -\frac{dC_{eq_{Ar}}}{dT}\frac{\dot{Q}}{C_P}, \qquad (3)$$

$$F_{N_2} = -\frac{dC_{eq_{N_2}}}{dT}\frac{\dot{Q}}{C_P}. \qquad (4)$$

Here, $F_{Ar}$ ($F_{N2}$) is the net sea-to-air Ar ($N_2$) flux in moles $m^{-2}$ $s^{-1}$, $dC_{eq\_Ar}$ ($dC_{eq\_N2}$) is the temperature derivatives of the
solubility of Ar ($N_2$) in mole $m^{-3}$ $K^{-1}$ (Weiss, 1970), $\dot{Q}$ is the net air-to-sea heat flux in J $m^{-2}$, and $C_P$ is the heat capacity of
180   seawater in J $m^{-3}$ $K^{-1}$. We boldly modeled the global ocean as 1-box and assumed an average temperature of 3.5 or 7.5 °C.
The temperatures of 3.5 and 7.5 °C, corresponding to the respective coefficients of $3.5\times10^{-23}$ (including deep water) and 3.0
$\times10^{-23}$ per meg $J^{-1}$ (not including deep water), were the average values of the ocean model shown in Fig. 1 of Bereiter et al.
(2018) for modern ocean. We also assumed constant $C_P$ and salinity of $3.9\times10^6$ J $m^{-3}$ $K^{-1}$ and 35 ‰, respectively. To convert
$F_{Ar}$ and $F_{N2}$ to changes in atmospheric $\delta(Ar/N_2)$, we employed $5.124\times10^{21}$ g for the total mass of dry air (Trenberth, 1981),
185   28.97 g $mol^{-1}$ for the mean molecular weight of dry air, $3.6\times10^{14}$ $m^2$ for the surface ocean area of the earth, and respective
fractions of 0.00933 and 0.7808 for Ar and $N_2$ in the atmosphere. As a result, the interannual variation in the global OHC
was estimated to drives only 10 % of the interannual variation in atmospheric $\delta(Ar/N_2)$. Although we do not fully understand
the basis of this discrepancy, it could be due to our treatment of the global ocean as a 1-box model and is thus too simplistic
to be used for an analysis of interannual variations and/or interannual variation in $\dot{Q}$ derived using the global OHC from the
190   NOAA/NCEI data is underestimated. In this regard, for seasonal to annual time scales, mixing in the atmosphere is

incomplete, as illustrated by the presence of a seasonal $\delta(Ar/N_2)$ cycle with opposite phase in the northern and southern hemispheres. Therefore, the local heat anomalies and atmospheric transport effects might have to be considered when interpreting interannual variability.

## 3.2 Simulation of gravitational separation and its effect on $\delta(Ar/N_2)$ at ground surface

As mentioned in Introduction, we have reported observational results of gravitational separation in the stratosphere (Ishidoya et al., 2008, 2013, 2018; Sugawara et al., 2018). Those results showed that stratospheric $\delta(Ar/N_2)$ also decreases rapidly with increasing altitude above the tropopause. Also, not only are there large year-to-year variations in the difference between the stratospheric and tropospheric $\delta(Ar/N_2)$ values, year-to-year variations in stratospheric $\delta(Ar/N_2)$ are much larger than those observed in the troposphere (Ishidoya et al., 2013; 2018). Therefore, we need to explore the possibility of tropospheric $\delta(Ar/N_2)$ variations caused by changes in gravitational separation. We have compared the observed and simulated gravitational separation of atmospheric major components above the tropopause in previous studies (Ishidoya et al., 2013, 2018; Sugawara et al., 2018; Belikov et al., 2019), but we did not consider gravitational separation in the troposphere. Therefore, in this study we improved the SOCRATES model to calculate variations in Ar and $N_2$ from the surface to 120 km, taking into account molecular diffusion processes generating gravitational separation. Here, we describe only those modifications we made to the model for the calculation of $\delta(Ar/N_2)$.

First, our 2-D model was expanded to be able to calculate explicitly any inert gas components and their isotopic ratios and elemental ratios, including $\delta(Ar/N_2)$. In our previous model studies, we used $^{44}CO_2$ and $^{45}CO_2$ to reproduce gravitational separation for the sake of simplicity. However, it is now necessary to explicitly include the molecular diffusion coefficients of all gas components in order to reproduce the molecular diffusion processes in the stratosphere more accurately, because the molecular diffusion coefficient is dependent on the molecular mass. In this study, the molecular diffusion coefficient of the gas component A in air ($D_A$) was calculated using the following equation (Poling, et al., 2001).

$$D_A = \frac{1.43 \times 10^{-4} T^{1.75}}{p\sqrt{m_{A-air}}\left(\sqrt[3]{\sigma_A} + \sqrt[3]{\sigma_{air}}\right)^2} \quad (5)$$

Here, $T$ and $p$ are the temperature (K) and pressure (hPa), respectively. $m_{A-air}$ is defined as follows.

$$\frac{1}{m_{A-air}} = \frac{1}{2}\left(\frac{1}{m_A} + \frac{1}{m_{air}}\right) \quad (6)$$

Here, $m_A$ and $m_{air}$ are the molecular mass number of component A and the mean mass number of air, respectively. $\sigma_A$ and $\sigma_{air}$ are the diffusion volumes of the component A and air, respectively. The diffusion volumes of $^{40}Ar$, $^{28}N_2$, and air are 16.2, 18.5, and 19.7, respectively (Poling et al, 2001).

Second, a new $\delta$ value has been defined and used for $\delta(Ar/N_2)$ in this study. Usually, the isotopic ratios or elemental ratios of the atmospheric major compositions are expressed as values relative to their ratios in the troposphere. Therefore, it is

common to treat the δ values at the ground surface as zero. However, high-precision analyses have recently revealed that, as is the case in δ(Ar/N₂), the δ values at the ground surface are not always constant, and they have seasonal and inter-annual variations, as well as long-term trends. The purpose of our analysis here is to evaluate the effect of gravitational separation on the δ value at the ground surface using the 2-D model. Therefore, it is no longer appropriate to assume that the δ value at

225    the ground surface is always zero. Observationally, small variations at the ground surface can be detected by using specific gas cylinders as constant references. In a numerical model, a constant reference is also needed for evaluating the effects of gravitational separation on the δ value at the ground surface. In our 2-D model, we used the ratio of total amount (M) of each gas component in the model atmosphere as the constant reference and defined a new δ value, $δ_Ω$, by the following equation.

$$\delta(Ar/N_2)_\Omega = \left( \frac{[n_{Ar}]\big/[n_{N_2}]}{M_{Ar}\big/M_{N_2}} - 1 \right) \times 10^6 \quad (7)$$

230    The total amount was calculated by integrating from the ground surface to the altitude of 120 km. According to this definition, $δ_Ω$ will be zero if there are neither molecular separations nor sinks/sources in the entire atmosphere. In the actual atmosphere, $δ_Ω$ becomes negative in the stratosphere due to gravitational separation, but will be a small positive value in the troposphere. A 50-year-long spin-up calculation was carried out for $δ(Ar/N_2)_Ω$ under steady-state condition, and we found that $δ(Ar/N_2)_Ω$ in the troposphere reached a steady-state value of about 30 per meg. In other words, the tropospheric $Ar/N_2$

235    ratio is enriched by about 30 per meg relative to the homogenous atmosphere due to the atmospheric gravitational separation. If the gravitational separation is strengthened due to atmospheric circulation changes in the stratosphere, $δ_Ω$ at the ground surface will slightly increase. On the other hand, if the gravitational separation is weakened in the stratosphere, $δ_Ω$ at the ground surface will decreases. Therefore, by using $δ_Ω$, it is possible to examine how a change in the gravitational separation in the stratosphere affects $δ_Ω$ at the ground surface.

240    Third, age of air (AoA) is calculated using a virtual tracer. In our previous model calculations, the AoA was calculated from the $CO_2$ mole fraction. However, since the actual increase in $CO_2$ mole fraction given at the ground surface is not a linear increase but includes non-linear trends and inter-annual fluctuations, it is not possible to estimate the correct AoA from the simple lag time method (e.g. Waugh and Hall, 2002). Therefore, in this study, we introduced an inert virtual tracer that increases linearly at the ground surface, and calculated the AoA in the stratosphere from the mole fraction of this virtual

245    tracer.

### 3.3 Long-term changes in the observed and simulated δ(Ar/N₂) and its implication for changes in OHC and BDC

To examine how $δ(Ar/N_2)_Ω$ is influenced by changes in the BDC, model simulations were made by arbitrarily changing the mean meridional circulation (MMC) represented by mass stream function in the 2-D model so that AoA changed by ±0.02 yrs yr$^{-1}$ at 35 km over the northern mid-latitudes. The simulated AoA values for the 35-km height are shown in Fig. 5. Here

250    the positive and negative increase rates correspond to the weakening and enhancement of the BDC simulations, respectively.

In this regard, Engel et al. (2009) reported an increase in AoA by $0.024\pm0.022$ yrs $yr^{-1}$ at the northern mid-latitudes in the middle stratosphere based on the observations of clock tracers such as $CO_2$ and $SF_6$, which is consistent with the weakened BDC simulation obtained in this study. On the other hand, previous studies using chemistry–climate models simulated a negative AoA trend between -0.005 and -0.02 yrs $yr^{-1}$ for the time period and location considered by Engel et al. (2009)

255   (Waugh, 2009). Therefore, the secular AoA trends obtained in our study fall within the range of those from clock tracers and climate models. However, recent studies (e.g. Ray et al., 2014) have reported increase and decrease of AoA in the middle and lower stratosphere, respectively, so that the uniform adjustment of mean meridional circulation in the present study is too simplistic to evaluate real changes in the BDC. Nevertheless, such simulation is worthwhile since it constitutes the first step to investigate the effect of gravitational separation of the whole atmosphere on the surface $\delta(Ar/N_2)$.

260   Secular changes in the simulated $\delta(Ar/N_2)_\Omega$ at the surface obtained from the weakened and enhanced BDC simulation, and those at 35 km are also shown in Fig. 5. As can be seen from the figure, clear seesaw relationships are found between the secular trends of $\delta(Ar/N_2)_\Omega$ at the surface and those at 35 km. In the weakened BDC simulation, $\delta(Ar/N_2)_\Omega$ changes secularly by 0.15 and -4.5 per meg $yr^{-1}$, respectively, at the surface and 35 km. In the enhanced BDC simulation, respective secular changes in $\delta(Ar/N_2)_\Omega$ by -0.13 and 4.0 per meg $yr^{-1}$ at the surface and 35 km are found. As discussed above, atmospheric

265   $\delta(Ar/N_2)$ increases by $3.5\times10^{-23}$ per meg when 1 J of heat is inputted into a 3.5 °C ocean water mass. Based on this relationship, when OHC increases by 100 ZJ during a 10-year period, which is comparable to the observed global 0 – 2000 m OHC increase during 2000 – 2010 (Levitus et al. 2012), the increase rate in atmospheric $\delta(Ar/N_2)$ is expected to be 0.35 per meg $yr^{-1}$. Therefore, 0.15 (-0.13) per meg $yr^{-1}$ for the surface $\delta(Ar/N_2)_\Omega$ due to the weakening (enhancement) of the BDC are non-negligible compared with the expected changes in atmospheric $\delta(Ar/N_2)$ due to the global OHC increase.

270   Figure 6 shows the observed $\delta(Ar/N_2)$ obtained at TKB, and its best-fit curve consisting of the fundamental and its first harmonics and a linear trend. The data are expressed as anomalies from the average value for the observation period. The linear trend is found to be $0.75\pm0.30$ per meg $yr^{-1}$, with respective uncertainties of $\pm0.11$ and $\pm0.28$ per meg $yr^{-1}$ for the regression and the stability of the standard air. We calculated an increase rate of $\delta(Ar/N_2)_{cor}$ by subtracting 0.15 per meg $yr^{-1}$ from $0.75\pm0.30$ per meg $yr^{-1}$ to remove the effects of $\delta(Ar/N_2)_\Omega$ increase obtained from the weakened BDC simulation. Thus,

275   derived secular increase rate of $\delta(Ar/N_2)_{cor}$, which represents the increase rate of $\delta(Ar/N_2)$ driven only by the OHC change, is $0.60\pm0.30$ per meg $yr^{-1}$. We can convert this increase rate to the global OHC increase rate by assuming above-mentioned coefficient of 3.5 (3.0) $\times10^{-23}$ per meg $J^{-1}$ (hereafter referred to as the increase rate of "$OHC_{ArN2}$"). The obtained secular increase of $OHC_{ArN2}$ by $17.1\pm8.6$ ($20.2\pm10$) ZJ $yr^{-1}$ is shown in Fig. 6, together with that of the global 0 – 2000 m OHC reported by NOAA/NCEI (hereafter referred to as "$OHC_{oc}$"). The increase rate of $OHC_{ArN2}$ is consistent with the $OHC_{oc}$

280   value of $12.2\pm1.2$ ZJ $yr^{-1}$ within uncertainties. Recently, by extracting a solubility-driven component of APO from their atmospheric $O_2/N_2$ ratio and $CO_2$ measurements and ocean model simulations, Resplandy et al. (2019) estimated an increase rate of the global OHC to be $12.9\pm7.9$ ZJ $yr^{-1}$ for the period 1991 – 2016 that is consistent, within the uncertainties, with the $OHC_{oc}$ during the same period. The results of the present study and Resplandy et al. (2019) suggest the usefulness of

atmospheric observations for independent confirmation of ocean heat uptake estimated from ocean temperature
285  measurements.

As described above, the increase rate in $OHC_{ArN2}$ obtained by using $\delta(Ar/N_2)_\Omega$ from the weakening BDC simulation agrees with the $OHC_{oc}$ estimate. On the other hand, the increase rate in $OHC_{ArN2}$ of 25.1±8.6 (29.6±10) ZJ yr$^{-1}$, obtained by using $\delta(Ar/N_2)_\Omega$ from enhanced BDC simulation assuming the coefficient of 3.5 (3.0) x10$^{-23}$ per meg J$^{-1}$, is significantly larger than the $OHC_{oc}$ estimate. In general, modeling studies have pointed to an accelerating BDC due to anthropogenic climate change
290  (e.g. Austin and Li, 2006). However, the increase rate in $OHC_{oc}$ agrees well $OHC_{ArN2}$ based on the weakened BDC simulation rather than on the enhanced BDC simulation. In this regard, several balloon-borne observations (Engel et al., 2009; Ray et al., 2014) and the ERA-Interim reanalysis data (e.g. Diallo et al., 2012) have suggested aging of air in the northern hemispheric midlatitude mid-stratosphere, implying a slowdown in the deep northern hemispheric branch of the BDC. Garfinkel et al. (2017) analyzed a series of chemistry-climate model experiments conducted for the period January
295  1960 through 2014. They found structural changes in BDC have occurred in the BDC since 1980s; BDC accelerated in the lower stratosphere in the northern hemisphere and tropics but not in the mid-stratosphere, and specifically since 1992, mean age increased by 0.12 year in the mid-stratosphere of the northern hemispheric mid-latitude and tropical mass upwelling has slowed down by 2 %. As discussed in our previous study (Sugawara et al., 2018), gravitational separation of the stratospheric air is sensitive to changes in mean meridional circulation rather than horizontal mixing. Therefore, it is thought
300  that the increase of mean age in the mid-stratosphere in the northern mid-latitude and the slowdown of tropical upwelling, suggested by the recent observational and modeling studies, are consistent with our weakened BDC simulation of the $\delta(Ar/N_2)_\Omega$.

We also carried out an additional simulation of $\delta(Ar/N_2)_\Omega$ considering the interannual variation in the BDC, to examine its effect on the large interannual variations of the observed $\delta(Ar/N_2)$ seen in Fig. 4. As the BDC interannual variation, we
305  simply assume a 10 % change in the MMC intensity with a 3-year cycle by changing the mass stream function in the 2-D model. Flury et al. (2013) reported that the speeds of BDC towards the NH and SH show interannual variabilities with amplitudes of about 21 and 10 %, respectively, and that the amplitude of variability in the ascent rate at the Equator is 21 %. Therefore, the 10% change in the MMC in our simulation is not an unrealistic assumption. As a result, the increase rate of $\delta(Ar/N_2)_\Omega$ showed an interannual variation with a peak-to-peak amplitude of ±0.4 per meg yr$^{-1}$. This interannual variation is
310  non-negligible but still rather small compared to that found in the observed $\delta(Ar/N_2)$, about ±4.5 per meg yr$^{-1}$, as seen from Fig. 4. Therefore, it is suggested that the interannual variation of surface $\delta(Ar/N_2)$ is driven mainly by solubility change in seawater and/or that the assumed ±10 % changes in the MMC intensity in our model is smaller than the actual interannual variation of the MMC. In addition, analytical artifacts and the extremely difficult challenge of maintaining stable standard air for $\delta(Ar/N_2)$ could also be cause(s) of the interannual variation. Therefore, further studies are needed to achieve quantitative
315  understanding of the discrepancy.

Consequently, if we regard OHC$_{oc}$ as representing "true" global OHC, then we can estimate secular trend and interannual variations in the BDC from $\delta$(Ar/N$_2$) observed at the surface. Conversely, if the simulated $\delta$(Ar/N$_2$)$_\Omega$ represents "true" BDC changes, then we can validate OHC$_{oc}$ by using OHC$_{ArN2}$. Therefore, the surface $\delta$(Ar/N$_2$) is found to be a unique tracer for changes in a spatiotemporally-integrated OHC and BDC. Not only longer-period precise observations of $\delta$(Ar/N$_2$), but also
320 improvements in $\delta$(Ar/N$_2$)$_\Omega$ simulation using 3-D atmospheric transport models are important future tasks.

## 4 Conclusions

We have been carrying out systematic measurements of atmospheric $\delta$(Ar/N$_2$) at TKB and HAT since 2012, COI and SYO since 2013 and 2016, respectively. Clear seasonal cycles of $\delta$(Ar/N$_2$) with summertime maximum were found at TKB, COI and SYO, with peak-to-peak amplitudes of 21±10, 11±4, 5±10 and 32±9 per meg at COI, TKB, HAT and SYO, respectively,
325 which are in general agreement with those observed at similar latitudinal sites by other investigators. The observed $\delta$(Ar/N$_2$) at TKB and HAT, after subtracting seasonal cycles and shorter-term variations, showed significant interannual variations and slight, but detectable, secularly increasing trends. The observed interannual variations correlated positively with that of the global OHC, suggesting a strong correlation between large-area air-sea heat flux and the long-term change in $\delta$(Ar/N$_2$). However, the ratio of interannual variation to secular increase is found to be much larger in $\delta$(Ar/N$_2$) than that in OHC, so
330 further studies are needed to interpret the discrepancy.

We improved the 2-D model we used in previous studies to calculate gravitational separation in order to evaluate its effect on the long-term change in the surface $\delta$(Ar/N$_2$). We simulated weakened and enhanced BDC by arbitrarily changing the MMC (represented by mass stream function in the model), and obtained effects of 0.15 and -0.13 per meg yr$^{-1}$, respectively, on the secular trend of the surface $\delta$(Ar/N$_2$). If we apply the correction for gravitational separation to the secular trend of
335 $\delta$(Ar/N$_2$) observed at TKB, then an average increase rate of 0.60±0.30 per meg yr$^{-1}$ for $\delta$(Ar/N$_2$) during 2012-2019 was obtained by assuming a weakening BDC. By using a conversion factor of 3.5 (3.0) x10$^{-23}$ per meg J$^{-1}$ by boldly assuming a 1-box ocean with a temperature of 3.5 (7.5) °C, we obtained an increase rate in the global OHC of 17.1±8.6 (20.2±10) ZJ yr$^{-1}$ for the 8-year period, which is consistent with 12.2±1.2 ZJ yr$^{-1}$ reported by NOAA/NCEI from the Argo float observations. On the other hand, the increase rate in the global OHC, obtained from the secular trend of $\delta$(Ar/N$_2$) at TKB under enhanced
340 BDC, was found to be significantly larger than that from the Argo float observations. These results indicate that the surface $\delta$(Ar/N$_2$) is a unique tracer for spatiotemporally-integrated OHC and BDC. Although an increase in global OHC is well known as an essential parameter to evaluate recent global warming, there is no method so far to validate OHC based on ocean temperature measurements. Long-term precise observations of $\delta$(Ar/N$_2$) will meet this demand, after correction for gravitational separation of the whole atmosphere.

345

*Data availability.*

The observational data of δ(Ar/N₂) presented in this study can be accessed by contacting the corresponding author.

*Author contributions.*

350 SI designed the study, carried out δ(Ar/N₂) measurements and drafted the manuscript. SS improved 2-D model and carried out δ(Ar/N₂)_Ω simulations. YT and DG managed the collections of air samples at Hateruma, Ochiishi, and Syowa station. KI examined the relationship of Ar and N₂ fluxes with air-sea heat flux. NA prepared gravimetric standard mixtures of Ar, O₂, N₂ and CO₂. SS, YT, DG, KI, YN, NA and SM examined the results and provided feedback on the manuscript. All the authors approved the final manuscript.

355

*Competing interests.*

The authors declare that they have no conflict of interest.

**Acknowledgements.**

360 We thank staff of Global Environmental Forum (GEF) and the Science Program of the Japan Antarctic Research Expedition (JARE) for their works to collect the air samples at Hateruma and Ochiishi stations (GEF) and Syowa station (JARE). This study was partly supported by the JSPS KAKENHI Grant Number 15H02814 and 18K01129, and the Global Environment Research Coordination System from the Ministry of the Environment.

**References**

365 Adachi Y, Kawamura K, Armi L, Keeling R. F.: Diffusive separation of the lower atmosphere. Science, 311, 1429, 2006.

Aoki, N., Ishidoya, S., Mastumoto, N., Watanabe, T., Shimosaka, T., and Murayama, S.: Preparation of primary standard mixtures for atmospheric oxygen measurements with uncertainty less than 1 ppm for oxygen mole fractions, Atmos. Meas. Tech., 12, 2631–2646, 2019.

Austin, J. and Li, F.: On the relationship between the strength of the Brewer–Dobson circulation and the age of stratospheric
370 air, Geophys. Res. Lett., 33, L17807, doi:10.1029/2006GL026867, 2006.

Belikov, D., Sugawara, S., Ishidoya, S., Hasebe, F., Maksyutov, S., Aoki, Morimoto, S., and Nakazawa, T.: Three-dimensional simulation of stratospheric gravitational separation using the NIES global atmospheric tracer transport model, Atmos. Chem. Phys., 19, 5349–5361, 2019.

Bereiter, B., Shackleton, S., Baggenstos, D., Kawamura, K., and Severinghaus, J.: Mean global ocean temperatures during
375 the last glacial transition, Nature, 553, 39–44, https://doi.org/10.1038/nature25152, 2018.

Blaine, T. W.: Continuous measurements of atmospheric argon/nitrogen as a tracer of air-sea heat flux: Models, methods, and data, Ph.D. thesis, Univ. of Calif., San Diego, La Jolla, 2005.

Blaine, T. W., Keeling, R. F. and Paplawsky, W. J.: An improved inlet for precisely measuring the atmospheric Ar/N₂ ratio,

Atmos. Chem. Phys. 6, 1181-1184, 2006.

380    Cassar, N., Mckinley, G. A., Bender, M. L., Mika, R. and Battle, M.: An improved comparison of atmospheric $Ar/N_2$ time series and paired ocean-atmosphere model predictions, J. Geophys. Res. 113, D21122, doi: 10.1029/2008JD009817, 2008.

Diallo, M., Legras, B., and Chédin, A.: Age of stratospheric air in the ERA-Interim, Atmos. Chem. Phys., 12, 12133–12154, https://doi.org/10.5194/acp-12-12133-2012, 2012.

Engel, A., Möbius, T., Bönisch, H., Schmidt, U., Heinz, R., Levin, I., Atlas, E., Aoki, S., Nakazawa, T., Sugawara, S., Moore,
385    F., Hurst, D., Elkins, J., Schauffler, S., Andrews, A., and Boering, K.: Age of stratospheric air unchanged within uncertainties over the past 30 years, Nature Geoscience, 2, 28–31, doi:10.1038/Ngeo388, 2009.

Flury, T., Wu, D. L., and Read, W. G.: Variability in the speed of the Brewer–Dobson circulation as observed by Aura/MLS, Atmos. Chem. Phys., 13, 4563–4575, 2013.

Garcia, H. and Keeling, R.: On the global oxygen anomaly and air-sea flux. J. Geophys. Res. 106 (C12), 31155-31166, 2001.

390    Garfinkel, C. I., Aquila, V., Waugh, D. W., and Oman, L. D.: Time-varying changes in the simulated structure of the Brewer–Dobson Circulation, Atmos. Chem. Phys., 17, 1313–1327, 2017.

Cheng, L., Abraham, J Hausfather, J. Z., Trenberth, K. E.: How fast are the oceans warming?, Science 363 (6423), 128-129, 2019.

Huang T, Walters S, Brasseur G, Hauglustaine D, Wu W.: Description of SOCRATES - A chemical dynamical radiative two-
395    dimensional model. NCAR/TN-440+EDD NCAR TECHNICAL NOTE, 1998.

Ishidoya, S., Sugawara, S., Morimoto, S., Aoki, S., and Nakazawa, T.: Gravitational separation of major atmospheric components of nitrogen and oxygen in the stratosphere, Geophys. Res. Lett., 35, L03811, doi:10.1029/2007GL030456, 2008.

Ishidoya, S., Sugawara, S., Morimoto, S., Aoki, S., Nakazawa, T., Honda, H., and Murayama, S.: Gravitational separation in
400    the stratosphere – a new indicator of atmospheric circulation, Atmos. Chem. Phys., 13, 8787–8796, 2013.

Ishidoya, S., and Murayama, S.: Development of high precision continuous measuring system of the atmospheric $O_2/N_2$ and $Ar/N_2$ ratios and its application to the observation in Tsukuba, Japan, Tellus 66B, 22574, http://dx.doi.org/10.3402/tellusb.v66.22574, 2014.

Ishidoya, S., Uchida, H., Sasano, D., Kosugi, N., Taguchi, S., Ishii, M., Morimoto, S., Tohjima, Y., Nishino, S., Murayama,
405    S., Aoki, S., Ishijima, K., Fujita, R., Goto, D., and Nakazawa, T.: Ship observations of Atmospheric Potential Oxygen and regional air-sea $O_2$ flux in the Northern North Pacific and the Arctic Ocean, Tellus B, 68, 29972, https://doi.org/10.3402/tellusb.v68.29972, 2016.

Ishidoya, S., Sugawara, S., Inai, Y., Morimoto, S., Honda, H., Ikeda, C., Hashida, G., Machida, T., Tomikawa, Y., Toyoda, S., Goto, D., Aoki, S., and Nakazawa, T.: Gravitational separation of the stratospheric air over Syowa, Antarctica and its
410    connection with meteorological fields, Atmos. Sci. Lett., e857. https://doi.org/10.1002/asl.857, 2018.

Keeling, R. F., Blaine, T., Paplawsky, B., Katz, L., Atwood, C., and Brockwell, T.: Measurement of changes in atmospheric $Ar/N_2$ ratio using a rapid-switching, single-capillary mass spectrometer system, Tellus, 56B, 322–338, 2004.

Keeling, R. F., Bender, M. L., and Tans, P. P.: What atmospheric oxygen measurements can tell us about the global carbon cycle, Global Biogeochem. Cycles, 7, 37-67, 1993.

415 Levitus, S., Antonov, J. I., Boyer, T. P., Baranova, O. K., Garcia, H. E., Locarnini, R. A., Mishonov, A. V., Reagan, J. R., Seidov, D., Yarosh, E. S., and Zweng, M. M.: World ocean heat content and thermosteric sea level change (0–2000 m), 1955–2010, Geophys. Res. Lett., 39, L10603, doi:10.1029/2012GL051106, 2012.

Nakazawa, T., Ishizawa, M., Higuchi, K. and Trivett, N. B. A.: Two curve fitting methods applied to $CO_2$ flask data. Environmetrics. 8, 197-218, 1997.

420 Poling B. E., Prausnitz, J. M., O'Connell, J. P.: The Properties of Gases and Liquids, McGraw-Hill Education, Fifth ed., 2001.

Ray, E. A., Moore, F. L., Rosenlof, K. H., Davis, S. M., Sweeney, C., Tans, P., Wang, T., Elkins, J. W., Bönisch, H., Engel, A., and Sugawara, S.: Improving stratospheric transport trend analysis based on $SF_6$ and $CO_2$ measurements, J. Geophys. Res.-Atmos., 119, 14–110, 2014.

425 Resplandy, L., Keeling, R.F., Eddebbar, Y., Brooks, M., Wang, R., Bopp, L., Long, M. C., Dunne, J. P., Koeve, W., and Oschlies, A.: Quantification of ocean heat uptake from changes in atmospheric $O_2$ and $CO_2$ composition, Sci. Rep., 9, 20244, doi:10.1038/s41598-019-56490-z, 2019.

Sturm, P., Leuenberger, M., Valentino, F. L., Lehmann, B. and Ihly, B.: Measurements of $CO_2$, its isotopes, $O_2/N_2$, and $^{222}Rn$ at Bern, Switzerland, Atmos. Chem. Phys.6, 1991-2004, 2006.

430 Sugawara, S., Ishidoya, S., Aoki, S., Morimoto, S., Nakazawa, T., Toyoda, S., Inai, Y., Hasebe, F., Ikeda, C., Honda, H., Goto, D., Putri, F. A.: Age and gravitational separation of the stratospheric air over Indonesia. Atmos. Chem. Phys., 18, 1819-1833, https://doi.org/10.5194/acp-18-1819-2018, 2018.

Tohjima, Y., Mukai, H., Machida, T. and Nojiri, Y.: Gas-chromatographic measurements of the atmospheric oxygen/nitrogen ratio at Hateruma Island and Cape Ochi-Ishi, Japan, Geophys. Res. Lett. 30, 1653, 435 doi:10.1029/2003GL01782, 2003.

Tohjima, Y., Mukai, H., Machida, T., Hoshina, Y., and Shin-Ichiro Nakaoka, S.: Global carbon budgets estimated from atmospheric $O_2/N_2$ and $CO_2$ observations in the western Pacific region over a 15-year period, Atmos. Chem. Phys., 19, 9269–9285, 2019.

Trenberth, K. E.: Seasonal variations in global sea level pressure and the total mass of the atmosphere. J Geophys. Res., 440 86(C6), 5238-5246, 1981.

Trenberth, K. E. and Fasullo, J. T.: Tracking Earth's Energy, Science 328 (316), 2010.

Waugh, D.W., and Hall, T. M.: Age of stratospheric air: Theory, observations, and models. Rev. Geophys., 40, no. 4, 1010, doi:10.1029/2000RG000101, 2002.

Waugh, D.W.: The age of stratospheric air. Nature Geoscience, 2, news&views, 14-16, 2009.

445 Weiss, R. F.: The solubility of nitrogen, oxygen and argon in water and seawater, Deep-Sea Res., 17, 721-735, 1970.
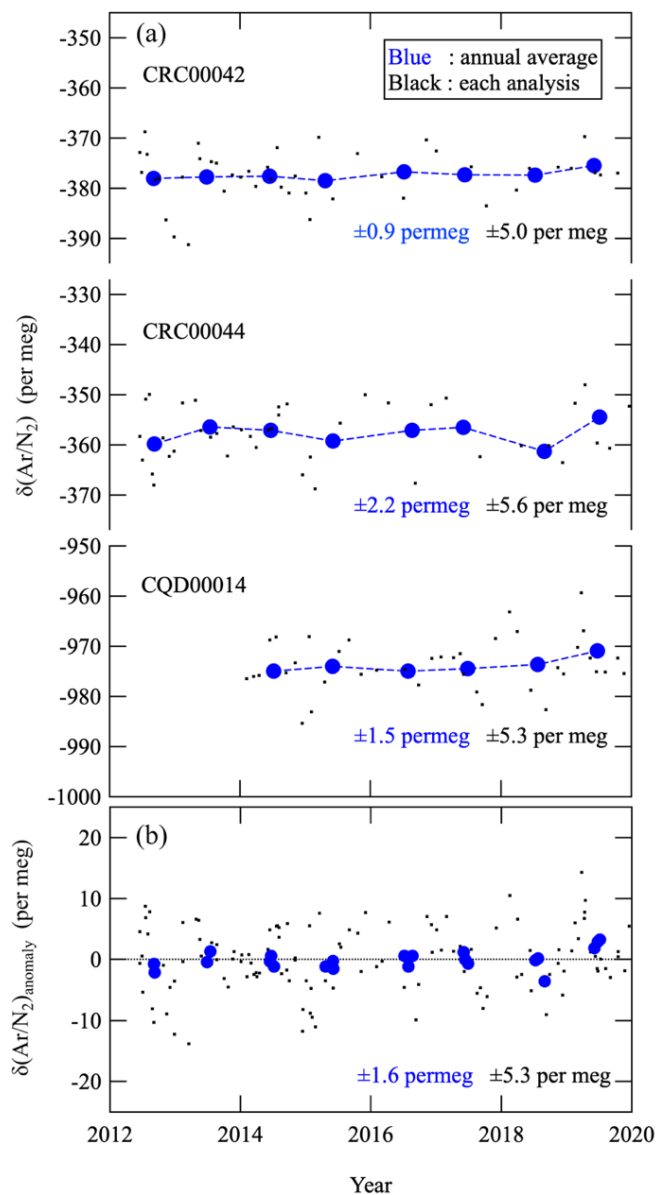
450

**Figure 1: (a) Each analysis value (black dots) and corresponding annual average (blue circles) of $\delta(Ar/N_2)$ of 3 standard air against the primary standard air. (b) Anomalies of $\delta(Ar/N_2)$ of 3 standard air shown in (a).**
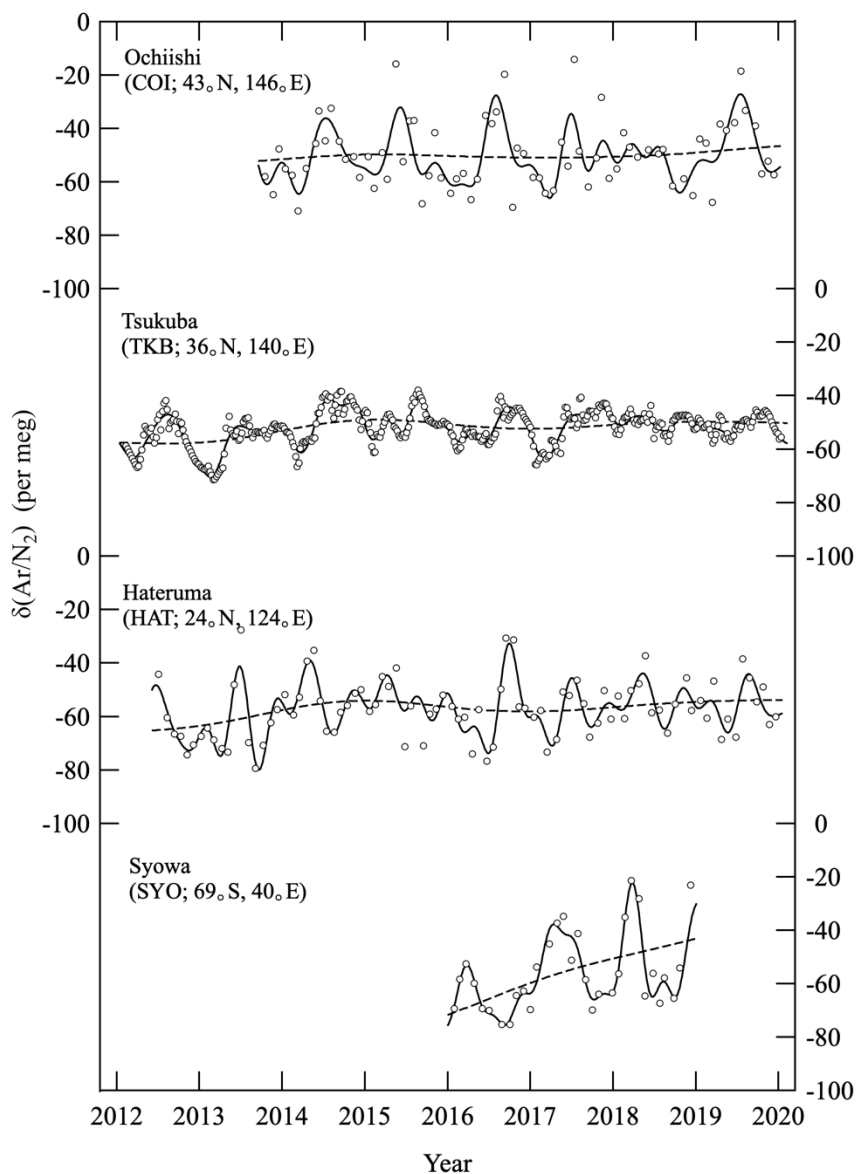
455

**Figure 2: Temporal variations of $\delta(Ar/N_2)$ at Ochiishi (COI), Tsukuba (TKB), and Hateruma (HAT), Japan and Syowa (SYO), Antarctica. Observed values are shown by open circles. Best-fit curves to the data (solid lines) and long-term trends (dashed lines) are also shown. All data are corrected for the scale drift of the primary standard air shown in Fig. 1 (b).**

460
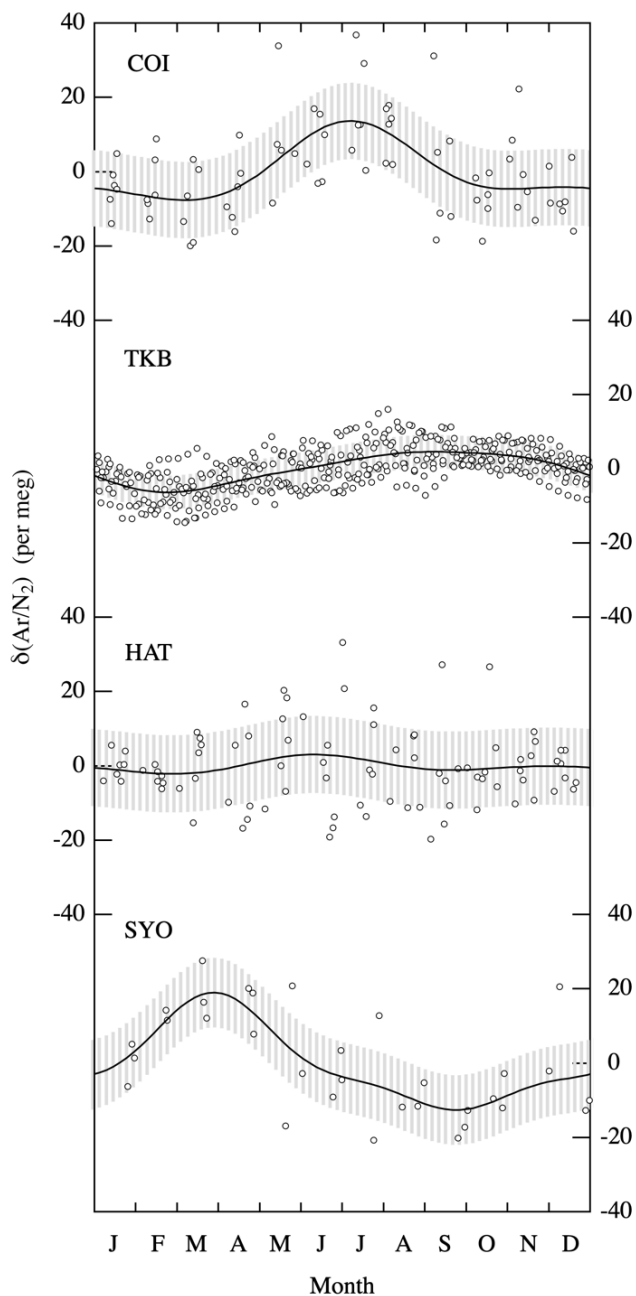
465

**Figure 3: Detrended values of δ(Ar/N₂) (open circles) and average seasonal cycles of δ(Ar/N₂) (solid lines) observed at COI, TKB, HAT and SYO. Gray shaded areas denote standard deviations of the detrended values from the average seasonal cycle at each site.**

470

Year
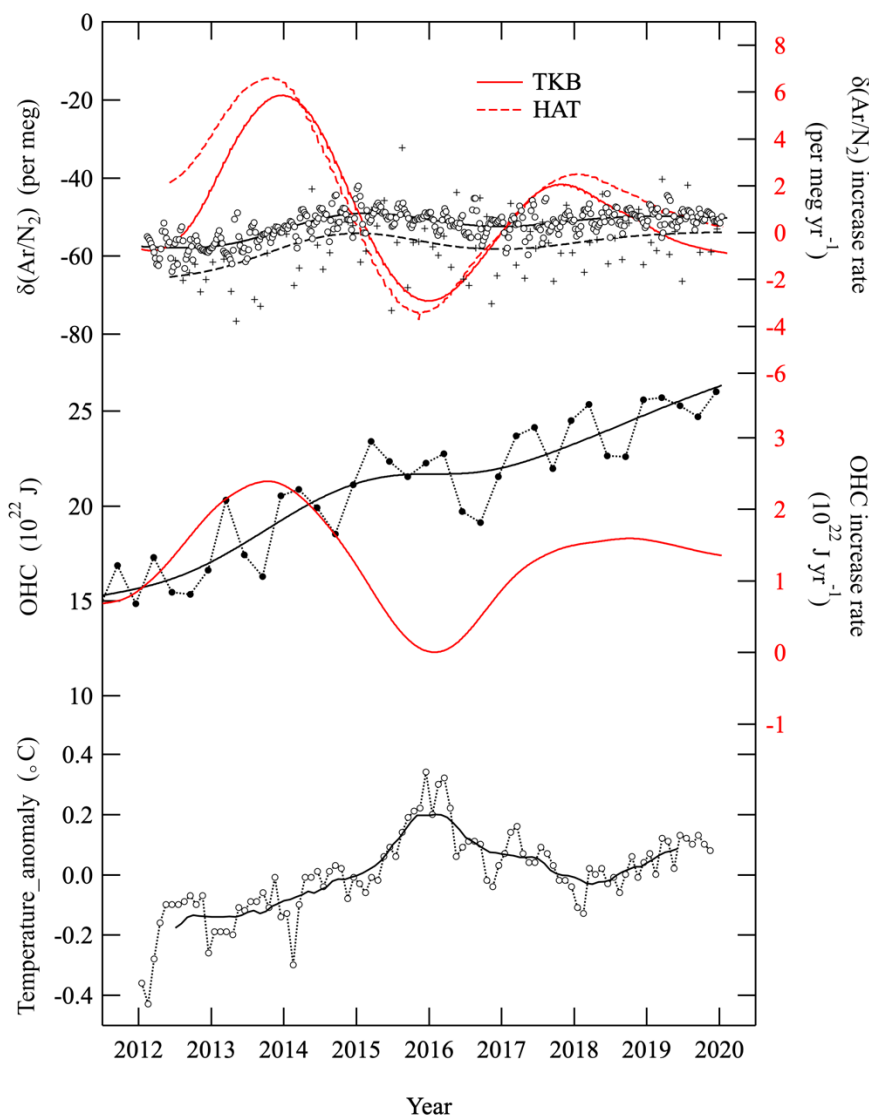
**Figure 4: (top)** δ(Ar/N₂) values at TKB (black open circles) and HAT (black crosses), after subtracting seasonal cycles and shorter-term variations less than 36 months. Long-term trends of δ(Ar/N₂) at TKB (black solid line) and HAT (black dashed line) are also shown. Increase rates of δ(Ar/N₂) at TKB and HAT are also shown by red solid and dashed lines, respectively. **(middle)** 0-2000 m global ocean heat content (OHC) from NOAA/NCEI (black filled circles), its long-term trend (black solid line) and increase rate (red solid line). **(bottom)** Global average surface temperature anomalies. Monthly and their 12-months running mean values are shown by open circles and solid line, respectively.

475

480
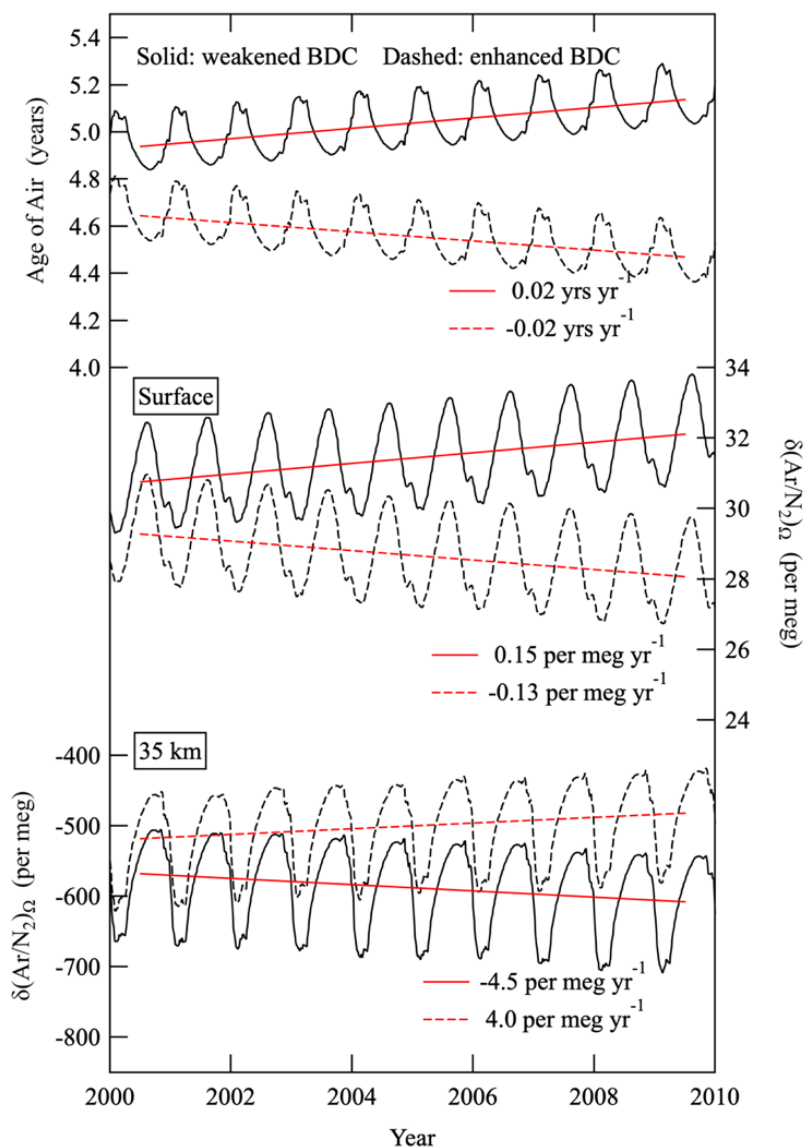
**Figure 5: Age of air (AoA) in the stratosphere at 35 km, $\delta(Ar/N_2)_\Omega$ at the surface and $\delta(Ar/N_2)_\Omega$ at 35 km simulated by using the SOCRATES 2-D model for weakened and enhanced BDC conditions (see text). Red solid and dashed lines denote secular trends of**
485   **$\delta(Ar/N_2)_\Omega$ for the weakened and enhanced BDC simulations, respectively, obtained by applying linear regression analyses to the annual average data.**

490
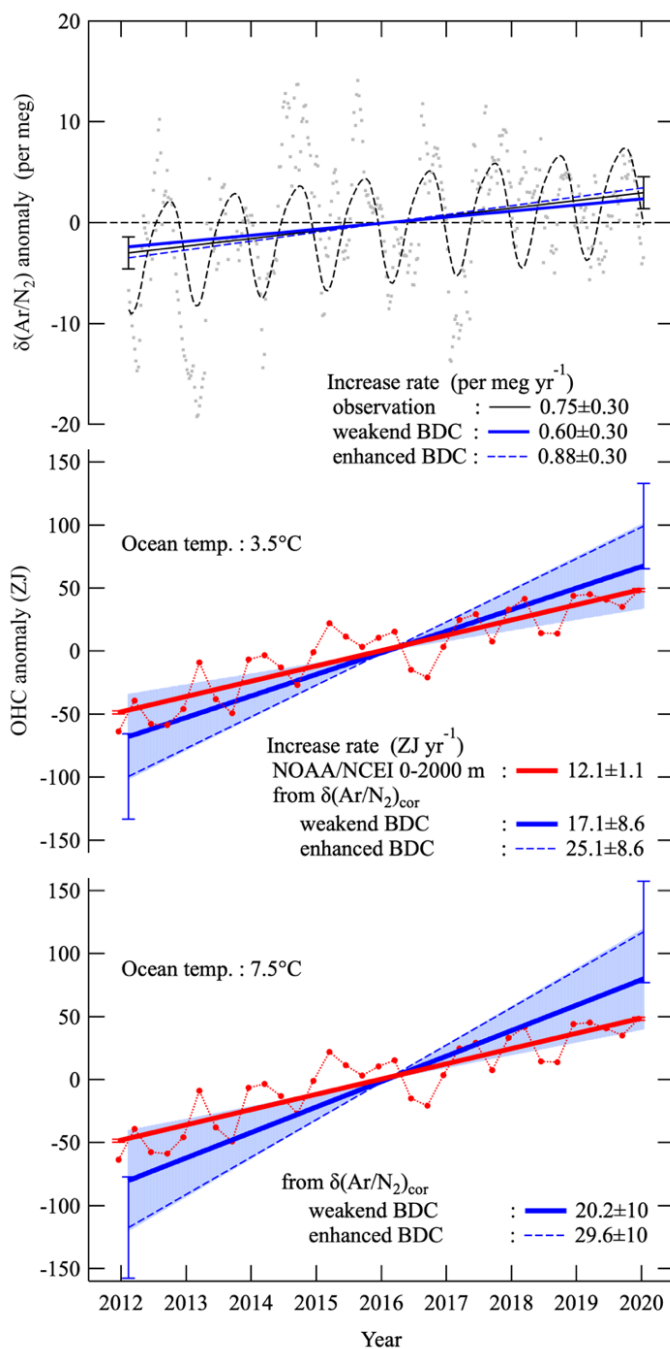
**Figure 6: (top) δ(Ar/N₂) observed at TKB (gray dots) and its best-fit curve consisting of the fundamental and its first harmonics and a linear trend (black dashed line). The linear trend is shown by a black solid line. Data are expressed as anomalies from the**

average value for the observation period. Thick blue and dashed blue lines denote the secular trends of $\delta(Ar/N_2)_{cor}$ derived by subtracting the secular trends of $\delta(Ar/N_2)_\Omega$ expected from weakened and enhanced BDC simulations, respectively, from the linear trend of $\delta(Ar/N_2)$ at TKB. (middle) Global OHC increase estimated from the secular trends of $\delta(Ar/N_2)_{cor}$ for weakened and enhanced BDC conditions (thick blue and dashed blue lines, respectively) using a conversion factor of $3.5 \times 10^{-23}$ per meg $J^{-1}$ by assuming a 1-box ocean with a temperature of 3.5 °C. Light blue shade and blue error bars denote the uncertainties of the OHC increases estimated from $\delta(Ar/N_2)_{cor}$ for weakened and enhanced BDC conditions, respectively. Red circles and the regression line denote the secular increase of 0-2000 m global OHC from NOAA/NCEI. (bottom) Same as in middle but for using a conversion factor of $3.0 \times 10^{-23}$ per meg $J^{-1}$ by assuming a 1-box ocean with a temperature of 7.5 °C.